Verification of an Automotive Headlight Leveling Circuit and Application Using Smart Component Property Extraction

Jérôme Kirscher,Michael Lenz,
Dieter Metzner, Georg Pelz
Infineon Technologies AG
Automotive Power
Am Campeon 1-12
D-85579 Neubiberg, Germany

Abstract

The paper discusses the simulative circuit verification of a power bridge in the context of its application, i.e. an automotive headlight leveling system. It especially emphasizes a topic, which is often neglected in mixed-domain modeling: the identification of the related component properties, e.g. the armature friction or torque constant of an electric motor. Typically, there are two ways to approach the problem: one is to scan the data sheets of the components. The other is to set up direct measurements of the component properties. The first approach opens a wide space, as the spec windows are often larger. The second requires substantial, additional effort. The paper offers a third opportunity, which relies on a measurement setup for system evaluation, which was available anyway.

1. INTRODUCTION

Today, the simulative verification of mechatronic systems, e.g. on the basis of languages like VHDL-AMS, gains more and more importance. One special observation is that the related circuit verification in a certain application context and the application verification itself are often in line with each other. Lots of papers have been written on model creation and application. We will also cover this topic, but will put an emphasis on another topic, that is often forgotten, i.e. the identification of the model parameters / component properties. Our focus is on an intelligent and cost-effective solution, which does not require much additional effort, but on the other hand allows to quickly and precisely reproduce measurement results in simulation, for further verification and exploration of the design space. This kind of parameter identification does not require any additional measurement provisions, apart from those to evaluate the system.

The application of the underlying methodology is shown using a real-life mechatronic application, an automotive headlight leveling system.

2. BEAM LEVELING

The purpose of beam length leveling is to prevent dazzling of oncoming traffic by headlights set too high. Such a situation may arrive when the back of a car is heavily loaded and thus the vehicle no longer horizontal. The headlight position has to be adapted to maintain optimum illumination of the road ahead.

The beam leveling is a Servo Control working as follows: the driver sets the reference value for the headlights on a potentiometer on the dashboard. The headlights are moved by a DC motor. A feedback potentiometer is connected to the motor shaft in such a way that the rotation of the shaft varies the value of the resistance so that the feedback voltage can be measured. The key component of the control circuit is the Integrated Circuit, which contains a full-bridge circuit (H-Bridge) to drive the motor and the complete logic necessary to compare the reference value with the feedback value. The motor is driven until these two values are virtually equal.
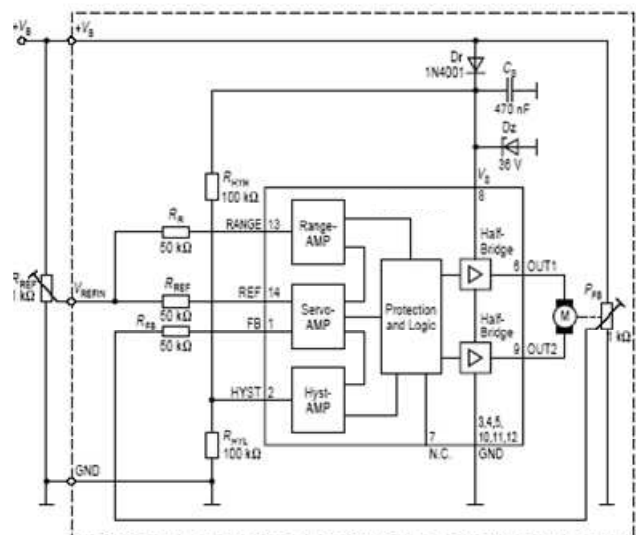

Figure. 1. Block diagram of a headlight leveling application.

Commonly in closed-loop circuit, oscillations can occur because the reference and feedback signals can never be exactly equal. In order to avoid this, a degree of *hysteresis* is introduced between these two signals (see Figure 2).

The headlight assembly has a certain mass. To avoid high mechanical stress, the braking of this mass is carried gently over a period of time. This region between braking and stopping is referred to as *deadband* (see Figure 2).
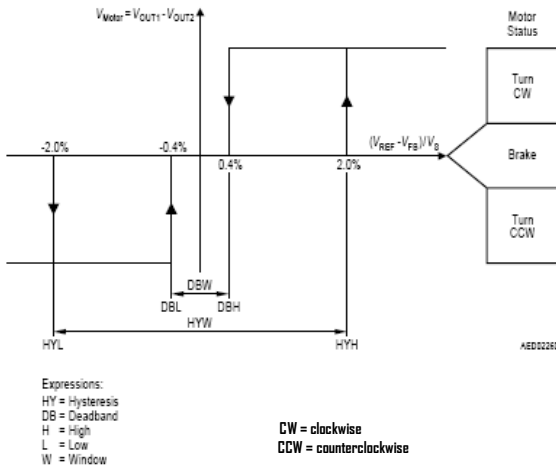

Figure. 2. Deadband and Hysteresis in the Servo principle.

3. REAL APPLICATION MODELING

The mechanical part of an automotive headlight leveling application comprises the following parts: DC motor, gear, potentiometer and the reflector.

For the modeling, friction and inertia are taken into account, and considered as part of the application.

The DC motor transforms the electrical energy into mechanical energy and the potentiometer changes its electrical resistance according the position of the reflector, thus we are speaking about an electromechanical system.
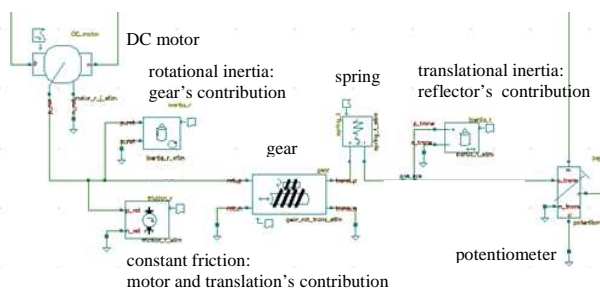

Figure. 3. Parts within the electromechanical application.

The DC motor shaft is connected to a gear, which consists of a pinion and a rack. The rack moves the reflector and the potentiometer. From a functional point a view, the gear performs a conversion between rotation (the pinion) and translation (the rack). Its rotational inertia is added as a separate contributor. The reflector's mass contribution is taken into account through its translational inertia extrapolated to the output of the gear. The contribution of the translational friction, together with an additional constant friction of the motor, is added at the output of the motor. A spring relates the elasticity in the system.

For each part, the electrical and mechanical conservation laws are explicitly formulated in its model's equations.

The models' parameters are summarized in Table 1.

Part	Parameters
DC motor	Armature resistance R
	Armature inductance L
	Torque constant Kt
	Back-emf constant Ke
	Damping D
	Moment of Inertia J
Constant friction	Friction $Tcst$, $Tcst = Tcst\_motor + Tcst\_system$
Gear inertia	Moment of Inertia Jg
Gear	Gear ratio *gear_ratio*
	Pinion radius *radius_p*
Spring	Spring constant Ks
Reflector inertia	Reflector's mass extrapolated to the output of the gear *mass_extrapolated*
Potentiometer	Factor k

Table. 1. List of the parameters involved in the models.

All these parameters are extracted from measurements and observations are performed on the real application.

The parameters extraction related to the DC motor is developed in details in the following section.

The model is based on classic electromechanical equations. The torque equation is described as follows:

$$T = -K_T \cdot i + D \cdot \omega + J \cdot \frac{d\omega}{dt} \qquad (1)$$

T is the torque produced by the motor. It is expressed as a function of the generated torque ($K_T i$) and the torque losses, $D.\omega$ (viscous damping loss) and $J.d\omega/dt$ (internal losses). The electrical equation is described as follows:

$$V = K_E \cdot \omega + R \cdot i + L \cdot \frac{di}{dt} \qquad (2)$$

V is the input voltage. It is equal to the sum of the back-emf ($K_E.\omega$), the motor's winding resistance voltage drop (R.i) and the winding inductance voltage drop (L.di/dt). If the standard units are used, $K_E = K_T$.

The winding inductance (L) is derived from the inrush current measurement (Figure 4.a). In this measurement the current flowing through the motor when the motor starts rotating, without load, is probed. The slope when the current starts rising from 0 A gives di/dt. At this very point $\omega = 0$ rad.s^{-1} and i = 0 A. U is read out and L is calculated, using Equation (2).

The winding resistance (R) is extracted from the oscillogram presented in Figure 4.b. In this measurement the rotor is blocked, so $\omega = 0$ rad.s^{-1}. When the steady state is reached, i is constant, so di/dt = 0 A.s^{-1}. U and i are read out from the oscillogram and R can be calculated, using Equation (2).

The back-emf coefficient (K_E) is derived from the measurement presented in Figure 4.c. In this measurement, the rotor is rotating at constant speed, without load, and the current flowing through the motor is probed. This constant angular velocity is computed out of the measurement, knowing that 4 current commutations correspond to one rotor rotation, and one rotation corresponds to 2π radian. This velocity has been named ω_{cst}. I is constant, so di/dt = 0 A.s^{-1} so K_E can be calculated using Equation (2). K_T is known as well, as $K_E = K_T$.

The moment of inertia (J) is extracted from the inrush current measurement (Figure 4.a). The angular acceleration $d\omega/dt$ is approximated from the measurement right at the start of the motor as follows: the first rotation duration is read out, knowing that 4 current commutations correspond to one rotor rotation, and then the angular velocity reached at the end of the first rotation is calculated. The average current flowing during this rotation is read out. As there is no load, T = 0 N.m and right at the beginning $\omega = 0$ rad.s^{-1}. As K_T is already known, Equation (1) gives J.

The damping coefficient (D) is derived from the coasting measurement (Figure 4.d). In this measurement, the battery is disconnected from the no-loaded motor and the internal losses slow the motor down. The voltage that remains on the motor connector is the one induced by the back-emf: it is a function of the angular velocity, and is equal to 0 when the rotor stops. During this parameter extraction, it has been figured out that a constant friction, i.e. independent of the angular velocity, was necessary to model the behavior observed in the measurements. This constant is named T_{cst_motor}. It is a part of the constant friction contributor (see Table 1). As there is no load, and no battery, T = 0 N.m and i = 0 A, and taking T_{cst_motor} into account, the equation (1) becomes:

$$0 = D \cdot \omega + J \cdot \frac{d\omega}{dt} + T_{cst\_motor} \qquad (3)$$

The angular deceleration (dω/dt) is approximated from the slopes traced on the oscillogram at the beginning and the end of the coasting phase, knowing that at the end $\omega = 0$ rad.s^{-1}, and at the beginning $\omega = \omega_{cst}$ (see K_E extraction). Equation (3) is then evaluated at these two points to first calculate T_{cst_motor} (Equation (4)), and then D (Equation (5)).

$$J \cdot \left(\frac{d\omega}{dt}\right)_2 = -T_{cst\_motor} \qquad (4)$$

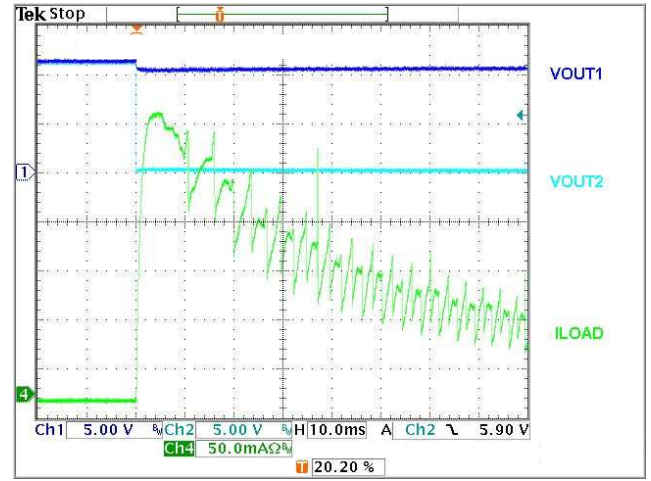$$J \cdot \left(\frac{d\omega}{dt}\right)_1 = -T_{cst\_motor} - D \cdot \omega_{cst} \qquad (5)$$

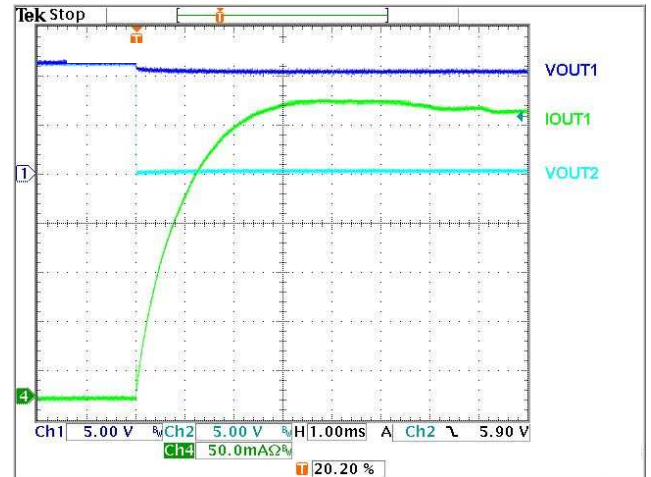**Figure. 4.a Inrush current -DC motor measurement.**

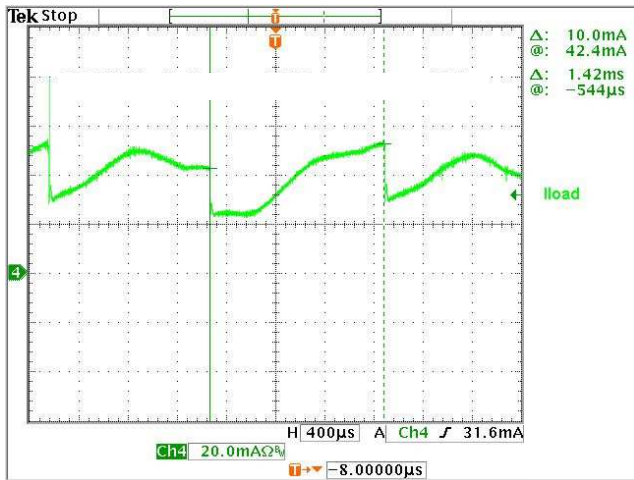**Figure. 4.b Rotor blocked -DC motor measurement.**

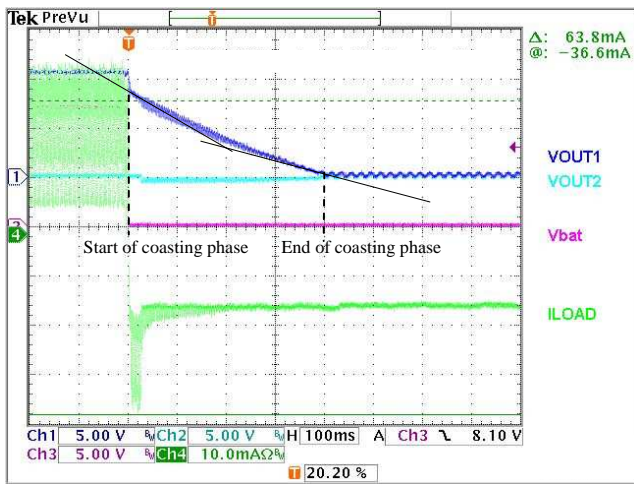**Figure. 4.c Constant speed rotation -DC motor measurement.**

Figure. 4.d Coasting phase -DC motor measurement.

4. SIMULATIONS

The main concern of the simulations is to reproduce the real conditions in which the Integrated Circuit would operate. The dash board passive components, the wiring harness losses as well as the external circuitry are integrated into the test bench by mean of VHDL-AMS models. The electromechanical system parts are the ones developed previously from measurements and observations performed on the real system application.

The transistor-level schematics of the Integrated Circuit are used in the Test-Bench (see Figure 5).
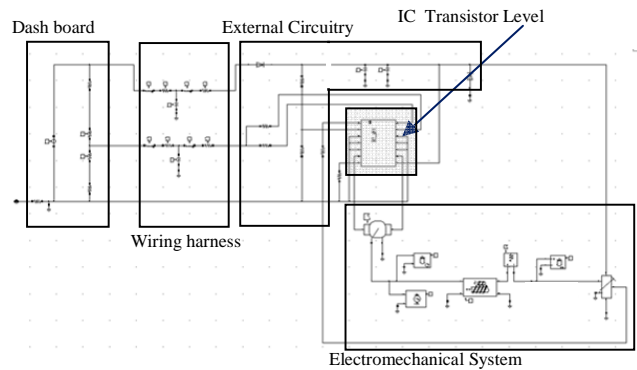

Figure. 5. Application Test-Bench.

Figures 6 show the typical tracking behavior of the servo system.

In Figure 6.a, the reference voltage, set by the user, and the feedback voltage are shown. The feedback voltage is directly proportional to the position of the reflector. As at the beginning of the simulation the position of the reflector is set to zero, the DC motor will rotate until the feedback voltage gets into the *deadband.* The frictions in the system are such that the Integrated Circuit manages stopping the reflector right at the lowest level of the *deadband.* At time   t = 3s, the reference voltage is increased with 1V, and again the DC motor starts rotating until the right position is reached.

Figure 6.b shows the voltages at the connectors of the DC motor model, which are forced by the H-Bridge. While the system is tracking the position imposed by the user, a difference voltage of 10.5V is set between the connectors of the motor model. When the Integrated Circuit stops the motor, it short circuits it with the supply voltage.
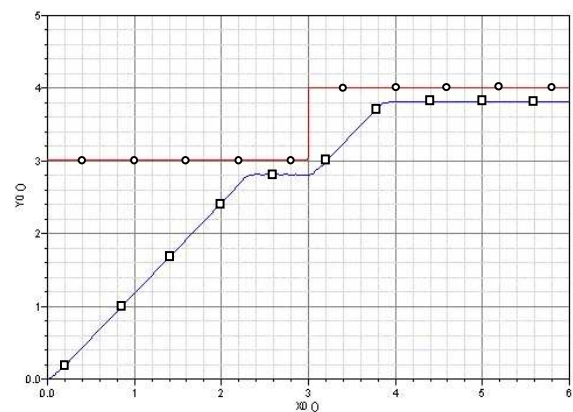

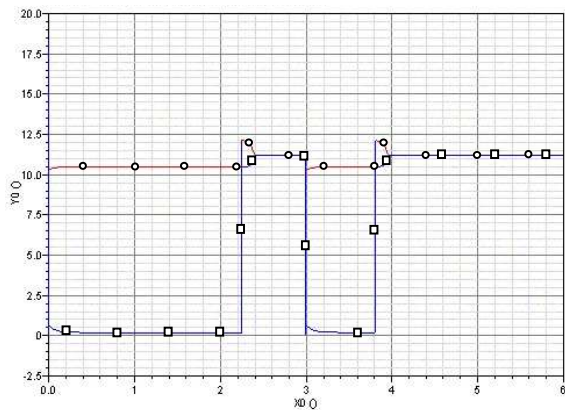**Figure. 6.a Reference (red ∘) and feedback (blue□) voltages -tracking simulation.**

Figure. 6.b DC motor's connector voltages (connector_1 voltage in blue ▫, connector_2 voltage in red ○) -tracking simulation.

Figure. 7.a Battery (blue ▫) and supply (red ○) voltages -overvoltage simulation.

Figures 7 show the Overvoltage Protection activation behavior.

In case of an overvoltage, the application can be over-loaded (e.g. the motor winding). To avoid this, the control circuit switches OFF the output stages to "High Impedance" if the supply voltage of the circuit reaches the overvoltage threshold *OVHI OFF*. The device switches on again when the supply voltage decreases to the *OVLO OFF* threshold, which is lower than the previous threshold. This hysteresis (*OV Hysteresis*) prevents ON-OFF oscillations, which might be caused by the wire harness inductive and resistive parasitics.

In Figure 7.a, battery and supply voltages are shown. The battery voltage is first ramped up from to 0V to 12V (phase 1), then from 12V to 24V and down to 12V again (phase 2) and finally ramped down from 12V to 0V (phase 3). As a diode is connected between the battery and the circuit supply pin, the supply voltage is 0.7V below the battery. In phases 1 and 3 the system is operating under normal conditions. At the beginning of the phase 2 the maximal supply voltage threshold *OVHI OFF* is exceeded and the circuit is in Overvoltage state. It remains in this state until the supply voltage decreases under the *OVLO OFF* threshold.

Figure 7.b shows the behavior of the voltages at the DC motor model connectors. In phases 1 and 3 the H-Bridge drives the motor and the connector_2 voltage follows the supply voltage. In phase 2 the H-Bridge out stages are deactivated and the DC motor is coasting: the voltages seen on the connectors are induced by the back-emf effect.
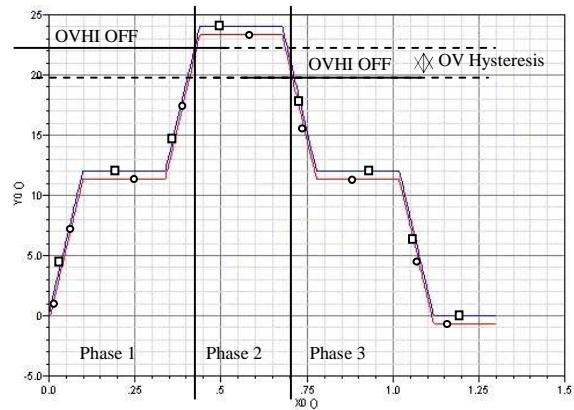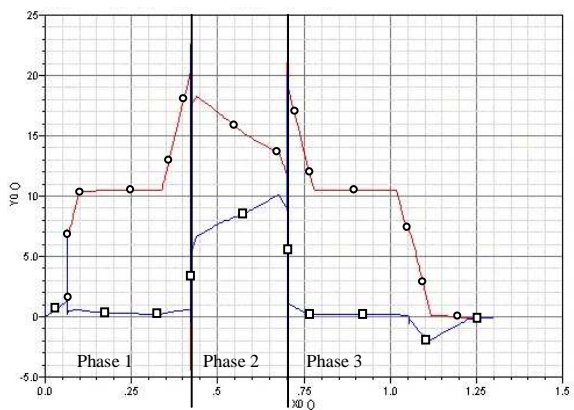

Figure. 7.b DC motor's connector voltages (connector_1 voltage in blue ▫, connector_2 voltage in red ○) -overvoltage simulation.

5. CONCLUSION

An intelligent and cost-effective solution to create application-based models has been shown. The use of these models to verify an Integrated Circuit in the context of its application has been illustrated, using the example of an H-Bridge Integrated Circuit, dedicated to level an automotive headlight beam. The benefits of such verification are numerous. It allows for instance the simulative verification of circuit design, as the transistor-level circuit can be simulated together with the models. New areas of the design can be explored, thanks to the flexibility of the models. Indeed, the extracted parameters can be adapted to perform worst-case simulations and test the robustness of the design. Moreover fast prototyping, with high reuse rate and short development cycle of an electromechanical application is possible, as all the processes are based on simulations and all the models' parameters can easily be changed. This is a must in the automotive industry.

6. REFERENCES

[1] *Georg Pelz:* "Mechatronics Systems – modeling and simulation with HDLs", John Wiley and Sons, 2003.

[2] *Douglas L. Perry:* Programming by Example. McGraw Hill. 2002

[3] *Richard J. Holleman:* IEEE Standard VHDL Analog and Mixed-Signal Extensions. Design Automation Standard Committee if the IEEE Computer Society. 1999.

[4] *Peter J. Ashenden, Gregory D. Perterson, Darrall A. Teegarden.* The System Designer's Guide to VHDL-AMS. Morgen Kaufmann Publisher. 2003

[5] *Mentor Graphics:* Fundamentals of VHDL-AMS for Automotive Electrical Systems. 2004

[6] *G. Pelz, J. Bielefeld und G. Zimmer:* „Modeling of Embedded Software for Automotive Applications", IEEE/VIUF Workshop on Behavioral Modeling and Simulation (BMAS), Washington D.C., 1997, 123-128.

[7] *J. Bielefeld, G. Pelz und G. Zimmer:* „AHDL-Model of a 2D Mechanical Finite-Element usable for Micro-Electro-Mechanical Systems", IEEE/VIUF Workshop on Behavioral Modeling and Simulation (BMAS), Washington D.C., 1997, 177-182.

[8] *G. Pelz, J. Bielefeld und G. Zimmer:* „Virtual Prototyping for a Camera Winder: a Case Study", IEEE/VIUF Workshop on Behavioral Modeling and Simulation (BMAS), Orlando, FL, 1998.

[9] *G. Pelz, T. Kowalewski, N. Pohlmann und G. Zimmer:* „Modeling of a Combustion Engine with Hardware Description Languages", IEEE/VIUF Workshop on Behavioral Modeling and Simulation (BMAS), Orlando, FL, 1998.

[10] *L. Voßkämper, A. Lüdecke, M. Leineweber und G. Pelz:* „Electromechanical Modeling Beyond VHDL-AMS", IEEE/ACM International Workshop on Behavioral Modeling and Simulation (BMAS), 1999.

[11] *A. Lüdecke, H.-K. Trieu, G. Hoffmann, P. Weyand und G. Pelz:* „Modeling in Hardware Description Languages for the Simulation of Coupled Fluidic, Thermal and Electrical Effects", IEEE/ACM International Workshop on Behavioral Modeling and Simulation (BMAS), 1999.

[12] *L.M. Voßkämper, R. Schmid und G. Pelz:* "Combining Models of Physical Effects for Describing Complex Electromechanical Devices", IEEE/ACM International Workshop on Behavioral Modeling and Simulation (BMAS), Orlando, Florida, USA, 2000.

[13] *D. Dammers, P. Binet, G. Pelz und L. Voßkämper:* "Motor modeling based on physical effect models", IEEE International Workshop on Behavioral Modeling and Simulation (BMAS) 2001.

[14] *G. Pelz:* "The Virtual Disk Drive - Mixed-domain support for disk electronics over the complete life-cycle", IEEE International Workshop on Behavioral Modeling and Simulation (BMAS) 2001.

[15] *D. Metzner, J. Schäfer und G. Pelz:* „HDL-Based System Engineering for Automotive Power Applications", IEEE International Workshop on Behavioral Modeling and Simulation (BMAS) 2003.

[16] *A. Pirker-Frühauf K. Schönherr, A. Laroche, G. Pelz:* „Worst-Case Modeling and Simulation of an Automotive Throttle in VHDL-AMS", IEEE International Workshop on Behavioral Modeling and Simulation (BMAS) 2007